SUPPLEMENTARY MATERIALS

Chirality without Stereoisomers: Insight from the Helical Response of Bond Electrons

Tianlv Xu[1], Xing Nie[1], Shuman Li[1], Yong Yang[1], Herbert Früchtl[2], Tanja van Mourik[2], Steven R. Kirk[*1], Martin J. Paterson[3], Yasuteru Shigeta[4] and Samantha Jenkins[*1]

[1]Key Laboratory of Chemical Biology and Traditional Chinese Medicine Research and Key Laboratory of Resource National and Local Joint Engineering Laboratory for New Petro-chemical Materials and Fine Utilization of Resources, College of Chemistry and Chemical Engineering, Hunan Normal University, Changsha, Hunan 410081, China

[2]EaStCHEM School of Chemistry, University of Saint Andrews, North Haugh, St Andrews, Fife KY16 9ST, Scotland, United Kingdom.

[3]Institute of Chemical Sciences, School of Engineering and Physical Sciences, Heriot-Watt University, Edinburgh, EH14 4AS, UK

[4]Center for Computational Sciences, University of Tsukuba, Tsukuba 305-8577, Japan

email: steven.kirk@cantab.net
email: samanthajsuman@gmail.com

1. Supplementary Materials S1. NG-QTAIM and stress tensor theoretical background and procedure to generate the stress tensor trajectories $\mathsf{T}_\sigma(s)$.

2. Supplementary Materials S2. $\mathsf{T}_\sigma(s)$ of the torsional C1-C2 *BCP* in the achiral S_N2 reaction.

3. Supplementary Materials S3. $\mathsf{T}_\sigma(s)$ of the torsional C1-C2 *BCP* in the chiral S_N2 reaction.

4. Supplementary Materials S4. $\mathsf{T}_\sigma(s)$ of the torsional C1-C2 *BCP* of ethane and substituted ethane.

5. Supplementary Materials S5. $\mathsf{T}_\sigma(s)$ of the torsional C1-C2 *BCP* of ethene and substituted ethene.

1. Supplementary Materials S1.

I(i) *QTAIM and stress tensor bond critical point (BCP) properties; ellipticity ε:*

The four types of QTAIM critical points are labeled using the notation (R, ω) where R is the rank of the Hessian matrix, i.e., the number of distinct non-zero eigenvalues and ω is the signature (the algebraic sum of the signs of the eigenvalues); the (3, -3) [nuclear critical point (*NCP*), a local maximum], (3, -1) and (3, 1) [saddle points, referred to as bond critical points (*BCP*) and ring critical points (*RCP*), respectively] and (3, 3) [the cage critical points (*CCP*)]. In the limit that the forces on the nuclei are zero, an atomic interaction line[Bader, R. F. W. A Bond Path: A Universal Indicator of Bonded Interactions. *J. Phys. Chem. A* **102**, 7314–7323 (1998)], the line passing through a *BCP* and terminating on two nuclear attractors along which the charge density $\rho(\mathbf{r})$ is locally maximal with respect to nearby lines, becomes a bond-path [Bader, R. F. W. Bond Paths Are Not Chemical Bonds. *J. Phys. Chem. A* **113**, 10391–10396 (2009)]. The full set of critical points with the bond-paths of a molecule or cluster is referred to as the molecular graph.

- Ellipticity $\varepsilon = |\lambda_1|/|\lambda_2| - 1$.

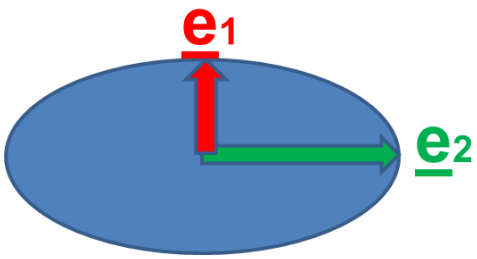

Scheme S1. The cross section through a bond at the bond critical point (*BCP*). The λ_1 and λ_2 eigenvalues with associated eigenvectors $\underline{\mathbf{e}}_1$ and $\underline{\mathbf{e}}_2$ respectively, define the axes of the ellipse and indicate the magnitudes of the least and greatest extents of the distribution of $\rho(\mathbf{r})$.

I(ii). *QTAIM bond-path properties; bond-path length (BPL), bond-path curvature, stress tensor eigenvalue $\lambda_{3\sigma}$ and the stress tensor trajectory $T_\sigma(s)$:*

The bond-path length (BPL) is defined as the length of the path traced out by the $\underline{\mathbf{e}}_3$ eigenvector of the Hessian of the total charge density $\rho(\mathbf{r})$, passing through the *BCP*, along which $\rho(\mathbf{r})$ is locally maximal with respect to any neighboring paths. The bond-path curvature separating two bonded nuclei is defined as the dimensionless ratio (BPL - GBL)/GBL, where the BPL is defined to be the bond-path length associated and GBL is the inter-nuclear separation. The BPL often exceeds the GBL particularly in strained bonding environments [Jenkins, S. & Heggie, M. I. Quantitative analysis of bonding in 90° partial dislocation in diamond. *J. Phys. Condens. Matter* **12**, 10325 (2000)]. Earlier, one of the current authors hypothesized that a bond-path may possess 1-D, 2-D or a 3-D morphology [*Chem. Phys. Lett.* **317,** 97–102 (2000)], with 2-D or a 3-D bond-paths associated with a *BCP* with ellipticity $\varepsilon > 0$, being due to the differing degrees of charge density accumulation, of the λ_2 and λ_1 eigenvalues respectively. Bond-paths possessing zero and non-zero values of the bond-path curvature defined by equation **(2)** can be considered to possess 1-D and 2-D topologies respectively. We start by choosing the length traced out in 3-D by the path swept by the tips of the scaled $\underline{\mathbf{e}}_2$ eigenvectors of the λ_2 eigenvalue, the scaling factor being chosen as the ellipticity ε, see **Scheme**

S1 (a).

- Stress tensor eigenvalue $\lambda_{3\sigma}$

This is used as a measure of bond-path instability, for values of $\lambda_{3\sigma} < 0$ and is calculated within the QTAIM partitioning.

The quantum stress tensor $\boldsymbol{\sigma}(\mathbf{r})$ is directly related to the Ehrenfest force by the virial theorem and therefore provides a physical explanation of the low frequency normal modes that accompany structural rearrangements [*Int. J. Quantum Chem.* **115,** 1678–1690 (2015).]. The form of the stress tensor, however, is ambiguous and consequently other forms of the stress tensor exist[36]. In this work we use the definition of the stress tensor proposed by Bader to investigate the stress tensor properties within QTAIM. [*J. Chem. Phys.* **73,** 2871–2883 (1980).]. The quantum stress tensor $\boldsymbol{\sigma}(\mathbf{r})$ is used to characterize the mechanics of the forces acting on the electron density distribution in open systems, defined as:

$$\boldsymbol{\sigma}(\mathbf{r}) = -\frac{1}{4}\left[\left(\frac{\partial^2}{\partial \mathbf{r}_i \partial \mathbf{r}'_j} + \frac{\partial^2}{\partial \mathbf{r}'_i \partial \mathbf{r}_j} - \frac{\partial^2}{\partial \mathbf{r}_i \partial \mathbf{r}_j} - \frac{\partial^2}{\partial \mathbf{r}'_i \partial \mathbf{r}'_j}\right) \cdot \gamma(\mathbf{r}, \mathbf{r}')\right]_{\mathbf{r}=\mathbf{r}'} \quad \textbf{(2)}$$

Where $\gamma(\mathbf{r},\mathbf{r}')$ is the one-body density matrix,

$$\gamma(\mathbf{r}, \mathbf{r}') = N \int \Psi(\mathbf{r}, \mathbf{r}_2, \dots, \mathbf{r}_N)\Psi^*(\mathbf{r}', \mathbf{r}_2, \dots, \mathbf{r}_N)\mathrm{d}\mathbf{r}_2 \cdots \mathrm{d}\mathbf{r}_N \quad \textbf{(3)}$$

The stress tensor is then any quantity $\boldsymbol{\sigma}(\mathbf{r})$, that satisfies equation **(2)** since one can add any divergence free tensor to the stress tensor without violating this definition [*J. Phys. Chem. A*, 2010, **114**, 8884–8895.], [*J. Phys. Chem. A*, 2011, **115**, 13001–13006.] [*J. Chem. Phys.*, 1980, **73**, 2871–2883.].

Earlier, it was found that the stress tensor trajectories $\mathsf{T}_\sigma(s)$ were in line with physical intuition [*Chem. Phys. Lett.* **667,** 25–31 (2017)].

If we first consider a tiny cube of fluid flowing in 3-D space the stress $\Pi(x, y, z, t)$, a rank-3 tensor field, has nine components [*Interdiscip. Appl. Math.* xxii,405 (2006).] of these the three diagonal components Π_{xx}, Π_{yy}, and Π_{zz} correspond to normal stress. A negative value for these normal components signifies a compression of the cube, conversely a positive value refers to pulling or tension, where more negative/positive values correspond to increased compression/tension of the cube. Diagonalization of the stress tensor $\boldsymbol{\sigma}(\mathbf{r})$, returns the principal electronic stresses Π_{xx}, Π_{yy}, and Π_{zz} that are realized as the stress tensor eigenvalues $\lambda_{1\sigma}$, $\lambda_{2\sigma}$, $\lambda_{3\sigma}$, with corresponding eigenvectors $\underline{\mathbf{e}}_{1\sigma}$, $\underline{\mathbf{e}}_{2\sigma}$, $\underline{\mathbf{e}}_{3\sigma}$ are calculated within the QTAIM partitioning.

Previously, $\lambda_{3\sigma}$ was used to detect the lowering of the symmetry, caused by a torsion about the central C-C bond in biphenyl, inducing a phase transition [*Int. J. Quantum Chem.* **115,** 1678–1690 (2015)]. The *BCP*s calculated with QTAIM and stress tensor partitionings will not always coincide, particularly under the application of external force, such as an applied torsion.

I(iii). *The stress tensor trajectory $\mathsf{T}_\sigma(s)$: background and interpretation*

The reason for subjecting a bond associated with a chiral carbon atom to a torsion distortion was to impose a symmetry breaking perturbation that sampled the most facile direction of torsion. The gap that we observe for the $\mathsf{T}_\sigma(s)$ between the CCW and CW torsions at a torsion $\theta = 0.0^o$ is due to their *BCP* shift vectors **dr** being oppositely directed and of non-zero magnitude. For example for a CCW torsion starting at $\theta = 0.0^o$ with a finite *BCP* shift **dr = {+0.01, 0.00, 0.00}**, the corresponding CW finite *BCP* shift **dr ≈ {-0.01, 0.00, 0.00},** giving a U_σ-space separation of the $\mathsf{T}_\sigma(s)$ of the CCW and CW torsions at a torsion $\theta = 0.0^o$ of approximately 0.01-(-0.01) = 0.02. This mapping is sufficiently symmetry breaking to enable the $\mathsf{T}_\sigma(s)$ of S and R stereoisomers at the equilibrium configuration to be distinguished, in contrast to conventional *scalar* QTAIM. The $\mathsf{T}_\sigma(s)$ comprises a series of contiguous points as a 3-D vector path displaying the effect of the structural change and is analyzed here in terms of the CW and CCW directions of bond torsion. The $\underline{\mathbf{e}}_{1\sigma}$ corresponds to the *most* preferred direction of charge density $\rho(\mathbf{r})$ accumulation and therefore the most facile direction in the plane perpendicular to the bond-path, where bond-torsion about the *BCP* does not involve structural distortion in the form of any increase in bond-path length from the straight-line bonded separation.

A value of $\{\underline{\mathbf{e}}_{1\sigma}\mathbf{.dr}\}_{\mathbf{max}} = 0.0$ corresponds to a constant orientation of the $\underline{\mathbf{e}}_{1\sigma}$ eigenvector in real space and therefore constant bond-path torsion (bond-twist). The subscript "$_{\mathbf{max}}$" corresponds to the difference between the minimum and maximum value of the projection of the *BCP* shift **dr** onto $\underline{\mathbf{e}}_{1\sigma}$ or $\underline{\mathbf{e}}_{2\sigma}$ or $\underline{\mathbf{e}}_{3\sigma}$ along the entire stress tensor trajectory $\mathsf{T}_\sigma(s)$, see **Tables 1-2**. We will denote the maximum stress tensor projections $\mathsf{T}_\sigma(s)_{max}$ = {bond-twist$_{max}$, bond-flexing$_{max}$, bond-anharmonicity$_{max}$}; these quantities therefore define the dimensions of a 'bounding box' around each $\mathsf{T}_\sigma(s)$.

The $\underline{\mathbf{e}}_{2\sigma}$ corresponds to the *least* preferred, i.e. the least readily distorted, direction of charge density $\rho(\mathbf{r})$ accumulation and therefore least facile direction in the plane perpendicular to the bond-path. This is because bond-flexing requires a greater structural distortion than bond-twist (torsion) in the form of an increase in bond-path length from the straight-line bonded separation. A value $\{\underline{\mathbf{e}}_{2\sigma}\mathbf{.dr}\}_{\mathbf{max}} = 0.0$ corresponds to constant bond-flexing in real space. A value of $\{\underline{\mathbf{e}}_{3\sigma}\mathbf{.dr}\}_{\mathbf{max}} > 0.0$ indicates the bond-anharmonicity corresponding to a changing *BCP* shift **dr** in real space relative to the bond-path, and therefore greater freedom for the *BCP* to slide along the bond-path; note the bond-anharmonicity axis label in **Figures 2**. Conversely, $\{\underline{\mathbf{e}}_{3\sigma}\mathbf{.dr}\}_{\mathbf{max}} = 0.0$ corresponds to a constant *BCP* shift **dr** in real space along the bond-path and therefore an absence of both displacement about the *BCP* and bond-anharmonicity.

The chirality-helicity measure $\mathsf{C}_{helicity}$ as a quantification of the chirality helicity equivalence

In this section, we explain the physical quantities used to define the *chirality-helicity* measure $\mathsf{C}_{helicity}$ using the stress tensor trajectory $\mathsf{T}_\sigma(s)$ as a result of the torsion of the bonds around a fixed reference atom (C1). A $\mathsf{T}_\sigma(s)$ with a non-zero value of the chirality-helicity measure $\mathsf{C}_{helicity}$ is formed from $\underline{\mathbf{e}}_{1\sigma}\mathbf{.dr}$ → bond-twist *BCP* displacement combined with *sufficient* axial displacement $\underline{\mathbf{e}}_{3\sigma}\mathbf{.dr}$ → bond-anharmonicity (*BCP* sliding)[65]. *BCP* sliding, the shift of *BCP* position along the containing bond-path, is due to changes to bonded

inter-nuclear separations. Note the use of the subscript "$_\sigma$" because C_σ is calculated using the stress tensor $T_\sigma(s)$. To be consistent with optical experiments as previously undertaken[29] we define S (left-handed) character to be dominant over R character (right-handed) for values of the chirality C_σ (CCW) > (CW) since CCW and CW represent left and right handed directions of torsion respectively. The chirality C_σ, is defined by the difference in the maximum $T_\sigma(s)$ projections (the dot product of the stress tensor $\mathbf{e_{1\sigma}}$ eigenvector and the *BCP* shift **dr**) of the $T_\sigma(s)$ values between the CCW and CW torsions:

$$C_\sigma = [(\mathbf{e_{1\sigma}}\cdot\mathbf{dr})_{max}]_{CCW} - [(\mathbf{e_{1\sigma}}\cdot\mathbf{dr})_{max}]_{CW}$$

These torsions correspond to the CW (-180.0° ≤ θ ≤ 0.0°) and CCW (0° ≤ θ ≤ 180.0°) directions of the torsion θ. The chirality C_σ quantifies the bond torsion direction CCW vs. CW, i.e. *circular* displacement, since $\mathbf{e_{1\sigma}}$ is the most preferred direction of charge density accumulation. The chiral asymmetry that we refer to as the helicity B_σ, defined as:

$$B_\sigma = [(\mathbf{e_{3\sigma}}\cdot\mathbf{dr})_{max}]_{CCW} - [(\mathbf{e_{3\sigma}}\cdot\mathbf{dr})_{max}]_{CW}$$

quantifies the direction of *axial* displacement of the bond critical point (*BCP*) in response to the bond torsion (CCW vs. CW), i.e. the sliding of the *BCP* along the bond-path[65]. The chirality-helicity measure $C_{helicity}$ = (chirality C_σ)×(helicity B_σ) = $C_\sigma B_\sigma$ is the simple arithmetic numerical product of the circular (C_σ) and axial (B_σ) displacement and consequently quantifies the displacement of the torsional *BCP* along the bond-path. The chirality-helicity measure $C_{helicity}$ describes values of $|C_{helicity}| > 0$ as a combination of circular displacement and axial displacement, where the net circular displacement (quantified by C_σ) occurs in the plane perpendicular to the net axial displacement (quantified by B_σ). The presence of helical displacement of the torsional *BCP* is determined by $B_\sigma \neq 0$, which may not necessarily coincide with helical shaped $T_\sigma(s)$, except for the limited case of conventionally chiral molecules such as lactic acid and alanine. The sign of the chirality determines the dominance of $\mathbf{S_\sigma}$ ($C_\sigma > 0$) and $\mathbf{R_\sigma}$ ($C_\sigma < 0$) character, see **Tables 1-2**. The helicity B_σ determines the dominance of $\mathbf{S_\sigma}$ or $\mathbf{R_\sigma}$ character with respect to the *BCP* sliding along the bond-path as a consequence of the bond-torsion. $B_\sigma > 0$ indicates dominant $\mathbf{S_\sigma}$ character and the converse is true for $B_\sigma < 0$.

I(iv). *The stress tensor trajectory $T_\sigma(s)$: numerical procedures to generate:*

The changing orientation and characteristics will be undertaken using the stress tensor trajectory space formalism of the bond critical points (*BCP*s). The stress tensor trajectory $T_\sigma(s)$ space U_σ has been previously used to track changing orientation and characteristics of the series of rotational isomers of the S and R stereoisomers of the lactic acid [*Journal of the American Chemical Society*, **141**(13), 5497–5503 (2019)], the prediction of torquoselectivity in competitive ring-opening reactions [*J. Comput. Chem.* **37,** 2722–2733 (2016)], elucidating the mechanism of photochromism and fatigue switches [*Int. J. Quantum Chem.* **118**(13),

e25565 (2018)], the functioning of doped azophenine switches [*Intl. J. Quantum. Chem.* **118**(16), e25676 (2018)] as well as for the reaction pathways of $(H_2O)_5$ [*Chem. Phys. Lett.* **667,** 25–31 (2017)]. The stress tensor trajectory $\mathsf{T}_\sigma(s)$ is intended for use in applications where there will be a finite, i.e. non-zero translation of a given *BCP*, either in real space or the stress tensor trajectory $\mathsf{T}_\sigma(s)$ space U_σ. For instance, previously, we examined torsion about the *BCP* located at the fixed 'pivot' of the torsion of the C-C bond linking the two phenyl rings in biphenyl where, as expected, was no significant translation of the central *BCP* [*Int. J. Quantum Chem.* **115,** 1678–1690 (2015)].

For a given *BCP*, the stress tensor eigenvectors $\{\underline{\mathbf{e}}_{1\sigma}, \underline{\mathbf{e}}_{2\sigma}, \underline{\mathbf{e}}_{3\sigma}\}$ for that *BCP* at the step of the normal mode displacement are used as the projection set for the entire stress tensor trajectory $\mathsf{T}_\sigma(s)$. The location in the stress tensor U_σ-space $\mathbf{dr}'(s)$ corresponding to the direction vector $\mathbf{dr}(s)$ in real space is given by $\{(\underline{\mathbf{e}}_{1\sigma}\cdot\mathbf{dr}), (\underline{\mathbf{e}}_{2\sigma}\cdot\mathbf{dr}), (\underline{\mathbf{e}}_{3\sigma}\cdot\mathbf{dr})\}$. The location in the U-space $\mathbf{dr}'(s)$ corresponding to the direction vector $\mathbf{dr}(s)$ in real space is given by $\{(\underline{\mathbf{e}}_{1}\cdot\mathbf{dr}), (\underline{\mathbf{e}}_{2}\cdot\mathbf{dr}), (\underline{\mathbf{e}}_{3}\cdot\mathbf{dr})\}$.

The explanation and numerical procedures for the stress tensor $\mathsf{T}_\sigma(s)$ trajectories.

The stress tensor trajectory $\mathsf{T}_\sigma(s)$ is constructed exclusively using the frame of reference defined by the eigenvectors $\{\pm\underline{\mathbf{e}}_{1\sigma},\pm\underline{\mathbf{e}}_{2\sigma},\pm\underline{\mathbf{e}}_{3\sigma}\}$ of the within the Hessian partitioning, of the total charge density $\rho(\mathbf{r_b})$ evaluated at the *BCP*, corresponding to the *equilibrium geometry* and is used to construct *all* subsequent points along the $\mathsf{T}_\sigma(s)$. This real space frame of reference has been referred to as U_σ-space [*J. Am. Chem. Soc.* **141**, 5497–5503 (2019)] [*Journal of Computational Chemistry* **410**(21), 1881-1891 (2019)] [*Chemical Physics Letters* **722**, 110–118, (2019)] [*Int J Quantum Chem* **118**(16) e25676 (2018).] [*Int J Quantum Chem* **118**(13), e25565 (2017)] [*Chem. Phys. Lett.* **667**, 25–31 (2017)] however, this nomenclature is unnecessarily complex and so we won't use it in the main text. The T_σ (s) is constructed using the change in position of the *BCP*, for all displacement steps **dr** of the *BCP* in the calculation. Each *BCP* shift vector **dr** is mapped to a point $\{(\underline{\mathbf{e}}_{1\sigma}\cdot\mathbf{dr}), (\underline{\mathbf{e}}_{2\sigma}\cdot\mathbf{dr}), (\underline{\mathbf{e}}_{3\sigma}\cdot\mathbf{dr})\}$ in sequence, forming the $\mathsf{T}_\sigma(s)$. This mapping is sufficiently symmetry breaking to distinguish stereo-isomers and isotopomers with degenerate relative energies. In contrast, *conventional* QTAIM is confined to the use of scalar measures and therefore can only magnify differences that may exist in relative energies associated with different structures. Conventional QTAIM cannot therefore distinguish stereo-isomers that have degenerate, i.e. equal, relative energies.

Numerical considerations for calculations of the trajectories:

Central to the concept of the trajectories $\mathsf{T}_\sigma(s)$ is the concept of a monotonically increasing sequence parameter s, which may take the form of an increasing integer sequence (0, 1, 2, 3,...) in applications where a set of discrete numbered steps are involved, or a continuous real number. The 3-D stress tensor trajectory $\mathsf{T}_\sigma(s)$ is then defined as an ordered set of points, whose sequence is described by the parameter s. In this application, we used an integer step number for s. We first choose to associate $s = 0$ with a specific reference molecular

graph, in this case, the energy minimum structure. For a specific *BCP*, the coordinates associated with each of the points are calculated by evaluating the components of the shift vector $\mathbf{dr} = \mathbf{r_b}(s) - \mathbf{r_b}(s\text{-}1)$ where $\mathbf{r_b}$ indicates the location of the *BCP*, from the previous step to the current step in the reference coordinate frame defined by the eigenvectors $\underline{\mathbf{e}}_{1\sigma}$, $\underline{\mathbf{e}}_{2\sigma}$, $\underline{\mathbf{e}}_{3\sigma}$.

Note: for displaying the QTAIM $\mathsf{T}(s)$ and stress tensor trajectories $\mathsf{T}_\sigma(s)$, large steps that can occur at the beginning or end of a stress tensor trajectory $\mathsf{T}_\sigma(s)$ may swamp the appearance of the stress tensor trajectory $\mathsf{T}_\sigma(s)$. To solve this we temporarily filter these steps before including them back in to correctly calculate the U_σ-space stress tensor trajectory $\mathsf{T}_\sigma(s)$.

The calculation of the $\mathsf{T}_\sigma(s)$ is made easier if the code which produces the list of structures corresponding to points along each step of the torsion (CW) ($-180.0^\circ \leq \theta \leq 0.0^\circ$) and counterclockwise CCW ($0.0^\circ \leq \theta \leq +180.0^\circ$) generates these structures at regularly-spaced points along. The consequence of this desirable characteristic is that there are few or no large changes or 'spikes' in the magnitude of the *BCP* shift vector **dr** i.e. $\Delta\mathbf{dr}$, between path step s and $s + 1$. Such anomalies occur because some path-following algorithms may employ occasional small predictor-corrector steps that are at least an order of magnitude smaller than standard steps. In this analysis it is observed that such intermittent relatively small steps in turn cause very small shifts **dr** to be interspersed between longer runs of larger changes, causing 'spike' noise in the otherwise smooth trajectories $\mathsf{T}(s)$. Such 'spikes', which usually only consist of a single spurious point deviating from the locally smooth stress tensor trajectory, can make potentially large spurious contributions to the stress tensor trajectory $\mathsf{T}_\sigma(s)$ and may be safely filtered. This filtering process was carried out manually in the current work.

In future to avoid the need to manually filter out these 'spikes', a combination of criteria are recommended for automated rejection of inclusion of a specific point into the trajectories $\mathsf{T}_\sigma(s)$:

1. If the magnitude of the **dr** associated with any current stress tensor trajectory point is less than 50% of the average of the corresponding **dr** values associated with the immediately preceding point and the immediately following point, the current point is filtered out as a 'spike'.
2. Abrupt changes in direction in the stress tensor trajectory $\mathsf{T}_\sigma(s)$, e.g. turning by more than 60^0 from one stress tensor trajectory $\mathsf{T}_\sigma(s)$ step to the next cause the current point to be labelled as a 'spike'.

These two rules taken together are referred to as the 'turn' filter. These rules can be repeatedly applied across multiple 'passes' through the stress tensor trajectory data as necessary.

It has been observed that the magnitudes of the steps **dr** naturally tend to slowly decrease toward the end of paths, corresponding to a slowed approach to an end minimum, and the corresponding part of the stress tensor trajectory $\mathsf{T}_\sigma(s)$ turns toward the U_σ-space origin. A combination of the criteria mentioned above may be deployed to retain these parts of the stress tensor trajectory $\mathsf{T}_\sigma(s)$.

An alternative Kolmogorov-Zurbenko (W. Yang and I. Zurbenko, ***WIREs Comp Stat***, 2010, **2**, 340–351) data smoothing filter may also be applied.

1. Percentage deviation $\Delta\mathbf{dr}$ of the magnitude of the **dr** from a moving average calculated along the stress tensor trajectory $\mathsf{T}_\sigma(s)$ exceeding a specific value should be 10% or less.
2. Abrupt changes in direction in the stress tensor trajectory $\mathsf{T}_\sigma(s)$, e.g. turning by more than 60^o from one stress tensor trajectory $\mathsf{T}_\sigma(s)$ step to the next.

It has been observed that the magnitudes of the steps **dr** naturally tend to slowly decrease toward the end of paths, corresponding to a slowed approach to an end minimum, and the corresponding part of the stress tensor trajectory $\mathsf{T}_\sigma(s)$ turns toward the U_σ-space origin. A combination of the criteria mentioned above may be deployed to retain these parts of the stress tensor trajectory $\mathsf{T}_\sigma(s)$. A range of alternative traditional 'denoising' algorithms may also conceivably be usefully deployed.

2. Supplementary Materials S2. $T_\sigma(s)$ of the torsional C1-C2 *BCP* in the S_N2 reaction of the attack of Br^- on monochloroethane.

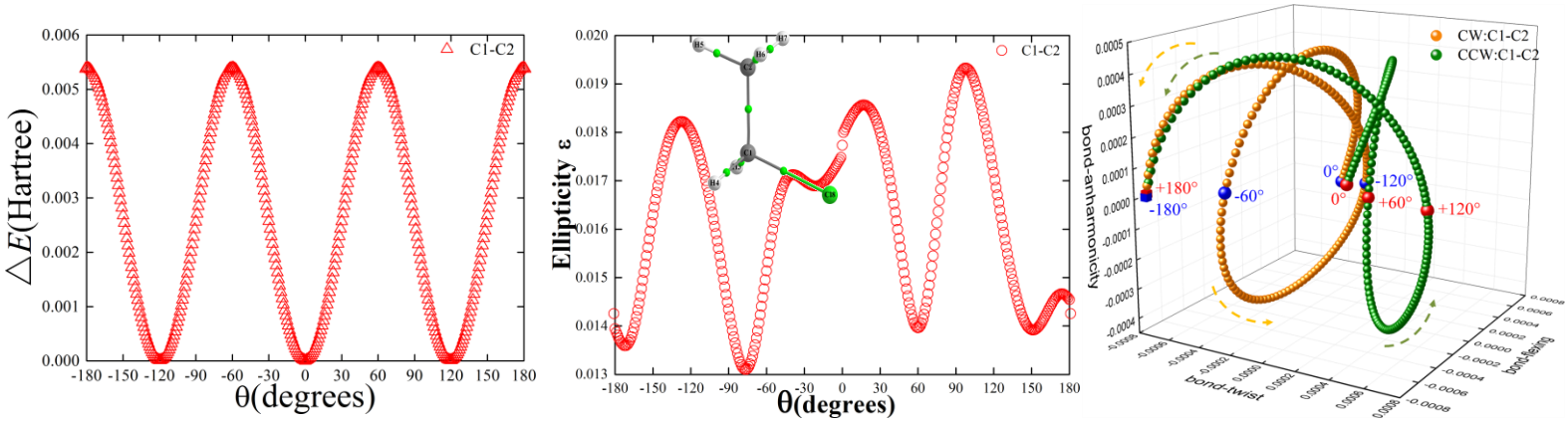

Figure S2(a): The variation of the relative energy ΔE (in a.u.) of monochloroethene (left panel) with the torsion θ, clockwise (CW) and counterclockwise (CCW) -180.0° ≤ θ ≤ +180.0° directions. The corresponding variation of the ellipticity ε (middle panel), with the monochloroethene molecular graph (inset panel) where the green spheres indicate the bond critical points (*BCP*s). The monochloroethene stress tensor trajectories $T_\sigma(s)$ (right panel) of the torsional C1-C2 *BCP* for the CW and CCW directions of torsion.

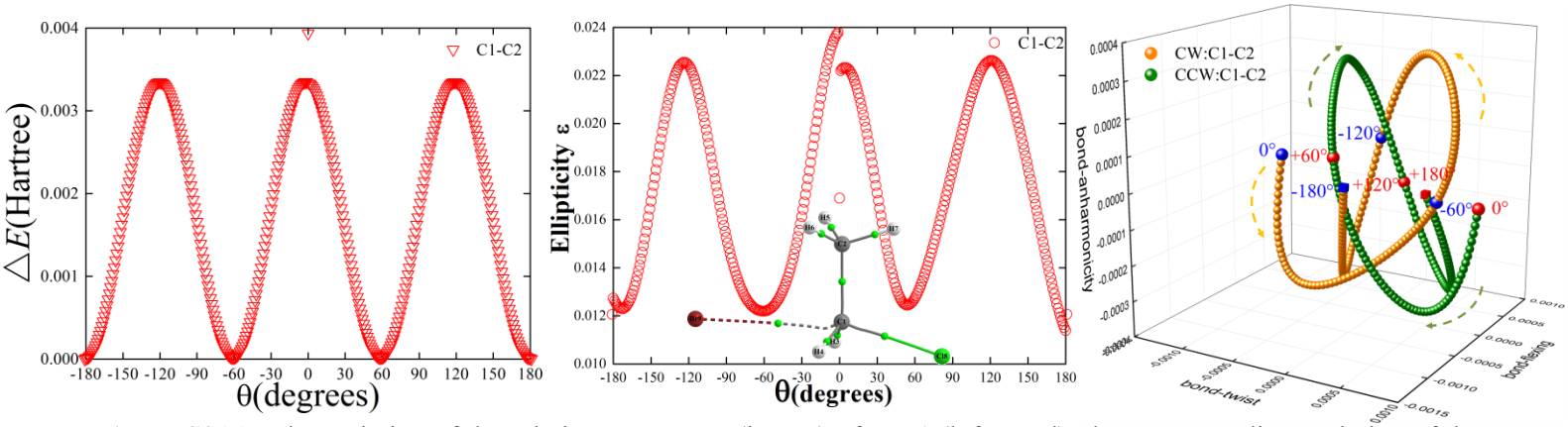

Figure S2(b): The variation of the relative energy ΔE (in a.u.) of INT1 (left panel), the corresponding variation of the ellipticity ε (middle panel), with the INT1 molecular graph (inset panel). The INT1 stress tensor trajectories $T_\sigma(s)$ (right panel) of the torsional C1-C2 *BCP*, see the caption of **Figure S2(a)**.

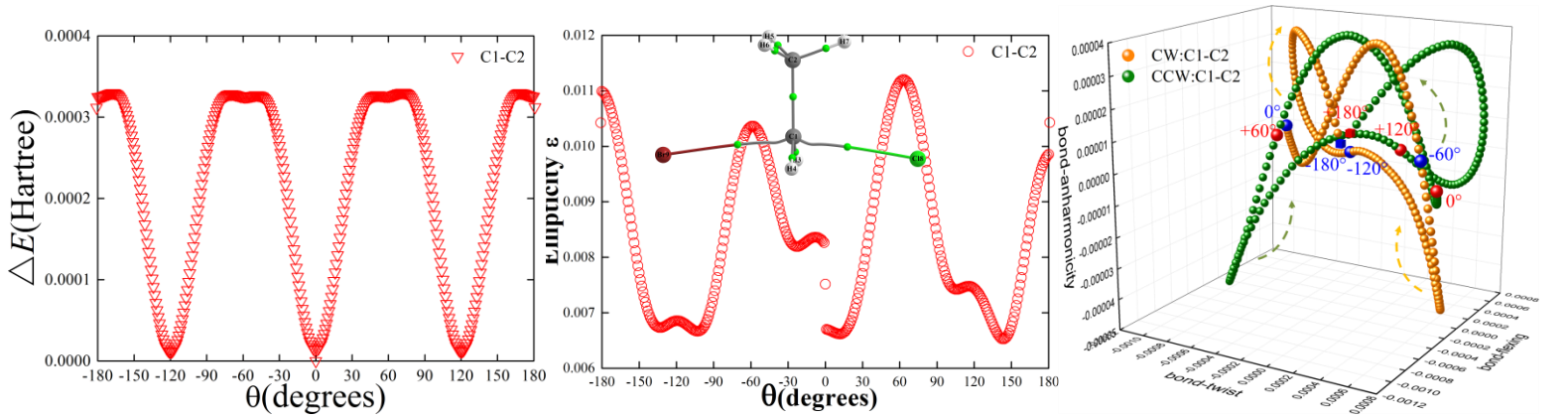

Figure S2(c): The variation of the relative energy ΔE (in a.u.) of the transition state (left panel) with the torsion θ. The corresponding variation of the ellipticity ε (middle panel), with the transition state molecular graph (inset panel). The Transition state $T_\sigma(s)$ (right panel) of the torsional C1-C2 *BCP*, see the caption of **Figure S2(a)**.

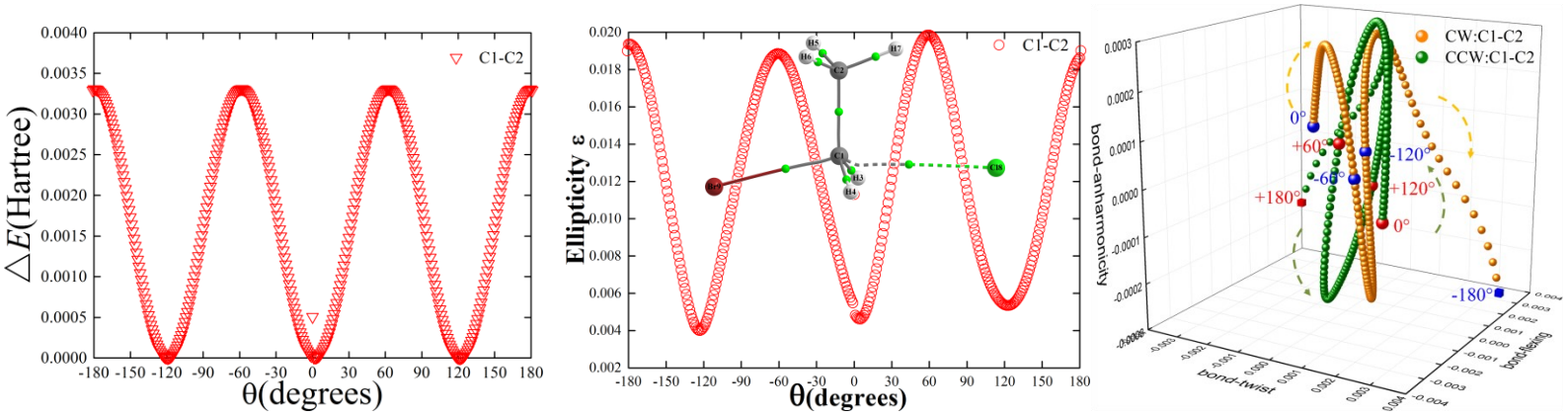

Figure S2(d): The variation of the relative energy ΔE (in a.u.) of INT2 (left panel). The corresponding variation of the ellipticity ε (middle panel), with the INT2 molecular graph (inset panel). The INT2 stress tensor trajectories $T_\sigma(s)$ (right panel) of the torsional C1-C2 *BCP*, see the caption of **Figure S2(a)**.

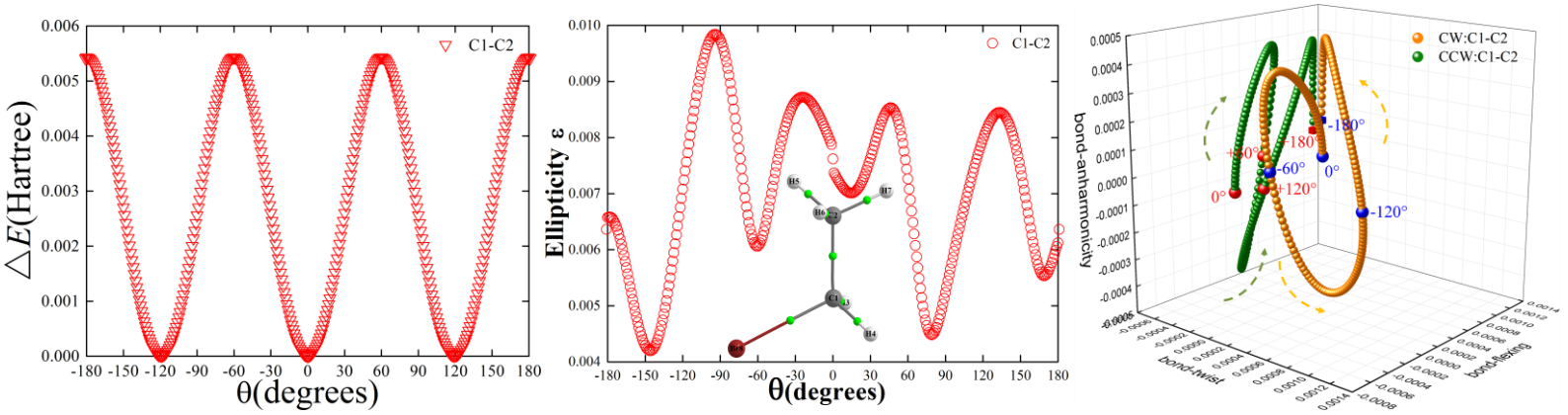

Figure S2(e): The variation of the relative energy ΔE (in a.u.) of monobromoethane (left panel) with the torsion θ. The corresponding variation of the ellipticity ε (middle panel), with the monobromoethane molecular graph (inset panel). The monobromoethane stress tensor trajectories $T_\sigma(s)$ (right panel) of the torsional C1-C2 *BCP*, see the caption of **Figure S2(a)**.

3. Supplementary Materials S3. $T_\sigma(s)$ of the torsional C1-C2 *BCP* in the S_N2 reaction of the attack of Br^-.

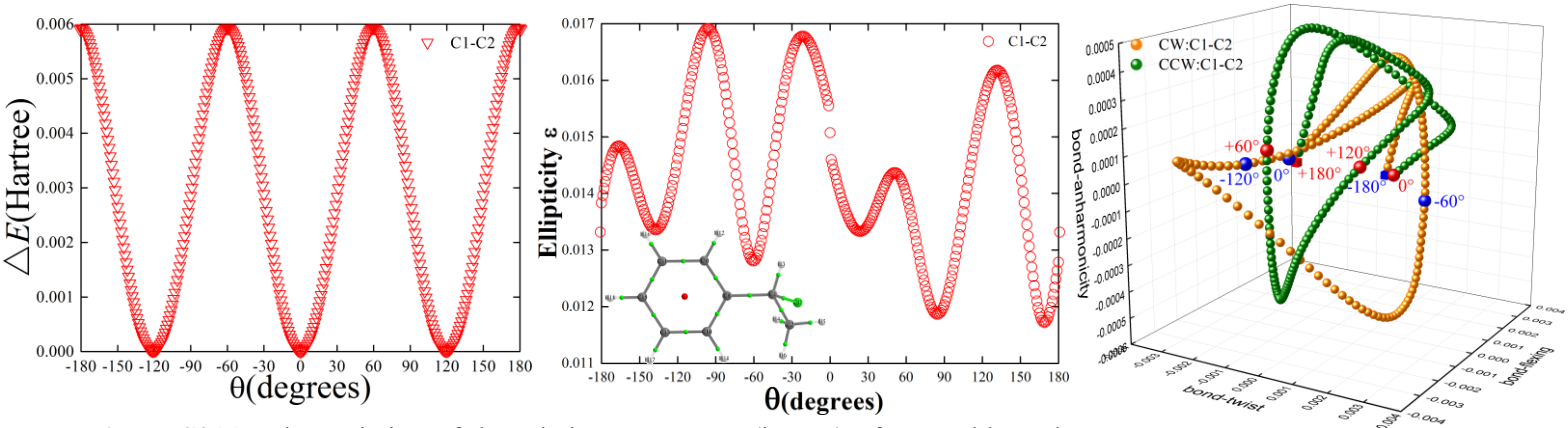

Figure S3(a): The variation of the relative energy ΔE (in a.u.) of monochloroethene (left panel) with the torsion θ, clockwise (CW) and counterclockwise (CCW) -180.0° ≤ θ ≤ +180.0° directions. The corresponding variation of the ellipticity ε (middle panel), with the monochloroethene molecular graph (inset panel) where the green spheres indicate the bond critical points (*BCP*s). The monochloroethene stress tensor trajectories $T_\sigma(s)$ (right panel) of the torsional C1-C2 *BCP* for the CW and CCW directions of torsion.

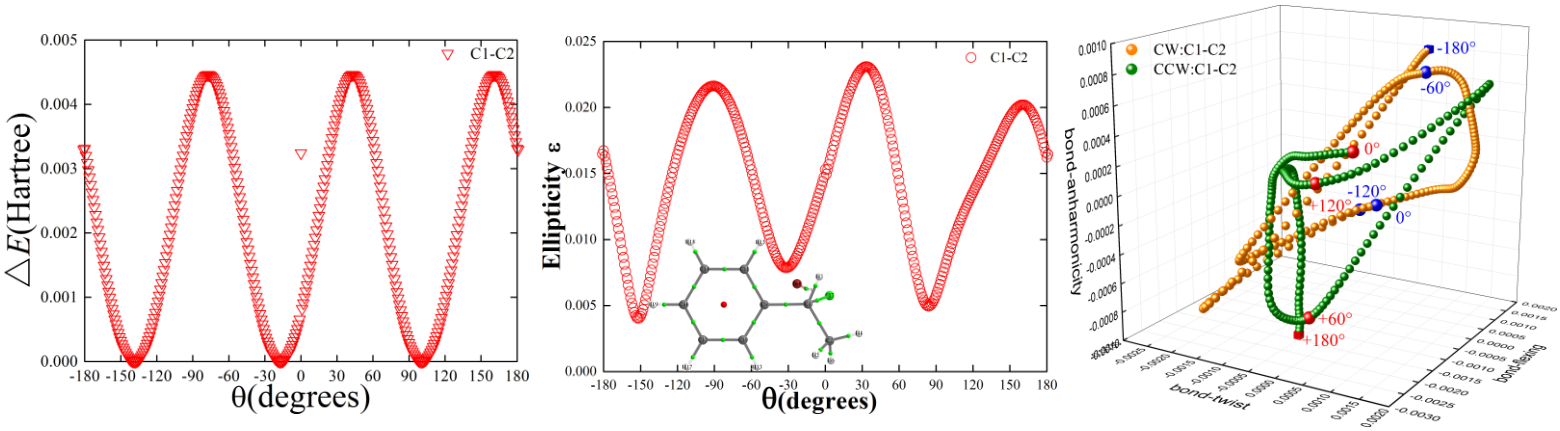

Figure S3(b): The variation of the relative energy ΔE (in a.u.) of INT1 (left panel). The corresponding variation of the ellipticity ε (middle panel), with the INT1 molecular graph (inset panel). The INT1 stress tensor trajectories $T_\sigma(s)$ (right panel) of the torsional C1-C2 *BCP*, see the caption of **Figure S3(a)**.

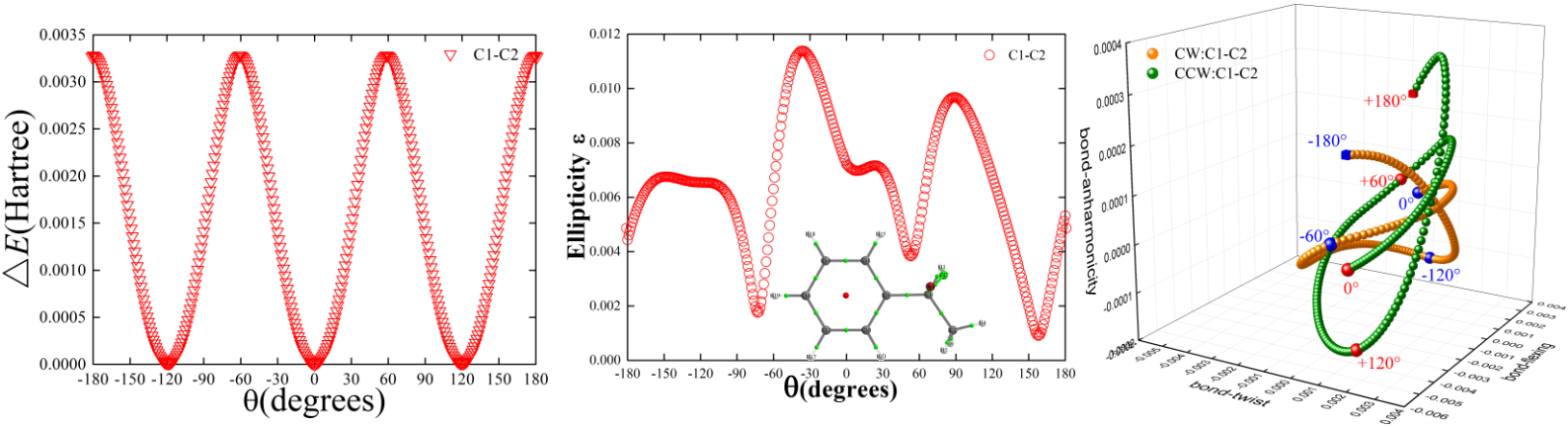

Figure S3(c): The variation of the relative energy ΔE (in a.u.) of transition state (left panel) with the torsion θ. The corresponding variation of the ellipticity ε (middle panel), with the transition state molecular graph (inset panel). The corresponding transition state $T_\sigma(s)$ (right panel) of the torsional C1-C2 *BCP*, see the caption of **Figure S3(a)**.

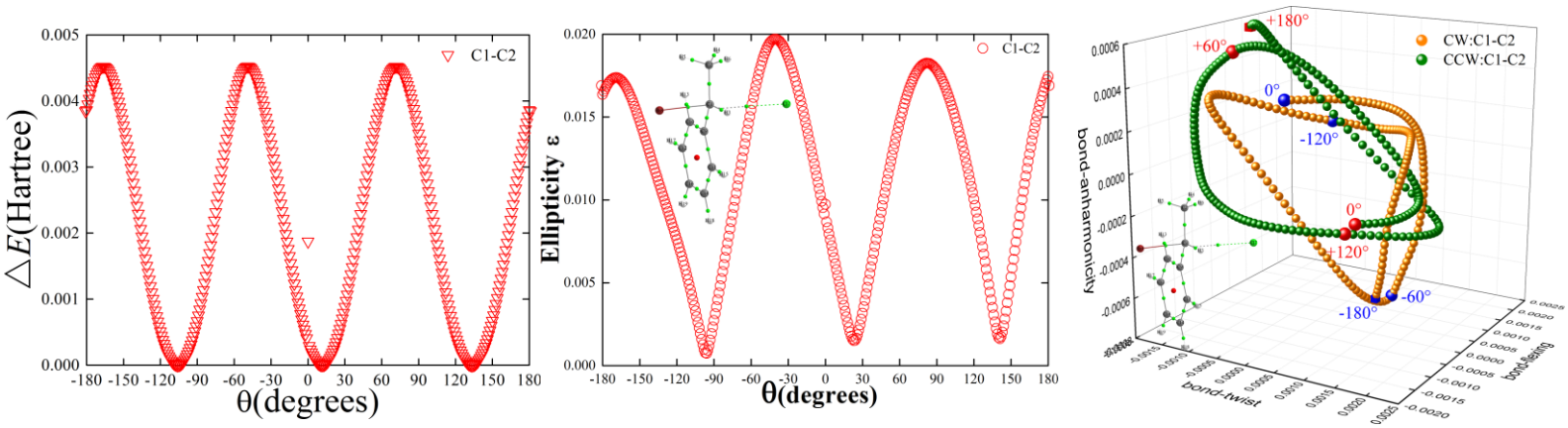

Figure S3(d): The variation of the relative energy ΔE (in a.u.) of INT2 (left panel). The corresponding variation of the ellipticity ε (middle panel), with the INT2 molecular graph (inset panel). The INT2 stress tensor trajectories $T_\sigma(s)$ (right panel) of the torsional C1-C2 *BCP*, see the caption of **Figure S3(a)**.

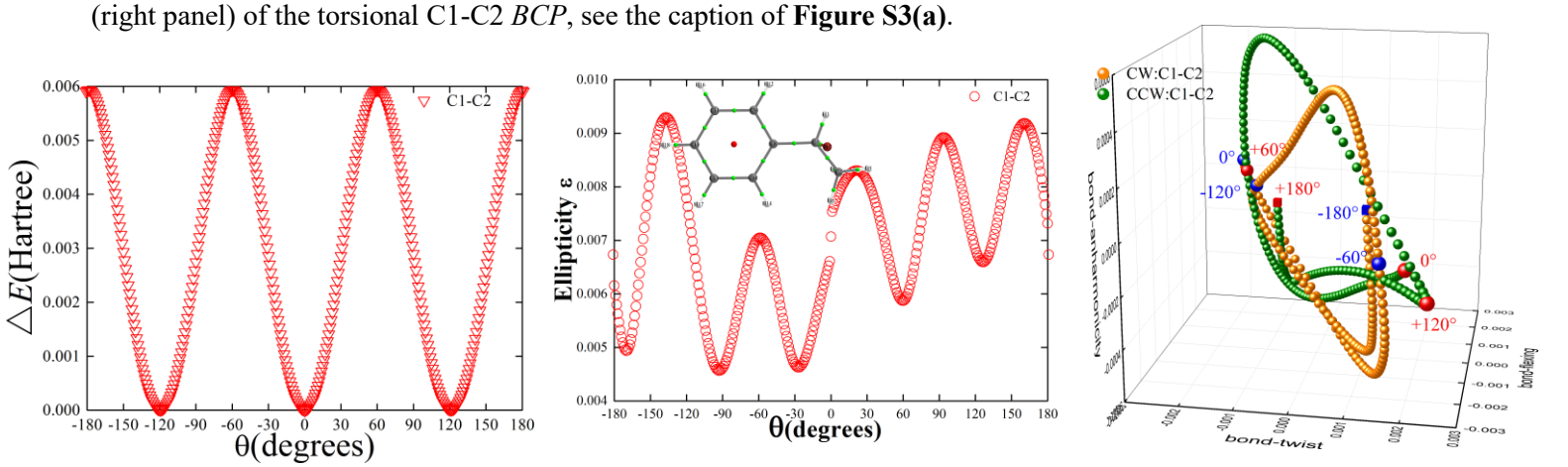

Figure S3(e): The variation of the relative energy ΔE (in a.u.) of monobromoethane (left panel) with the torsion θ. The corresponding variation of the ellipticity ε (middle panel), with the monobromoethane molecular graph (inset panel). The monobromoethane stress tensor trajectories $T_\sigma(s)$ (right panel) of the torsional C1-C2 *BCP*, see the caption of **Figure S3(a)**.

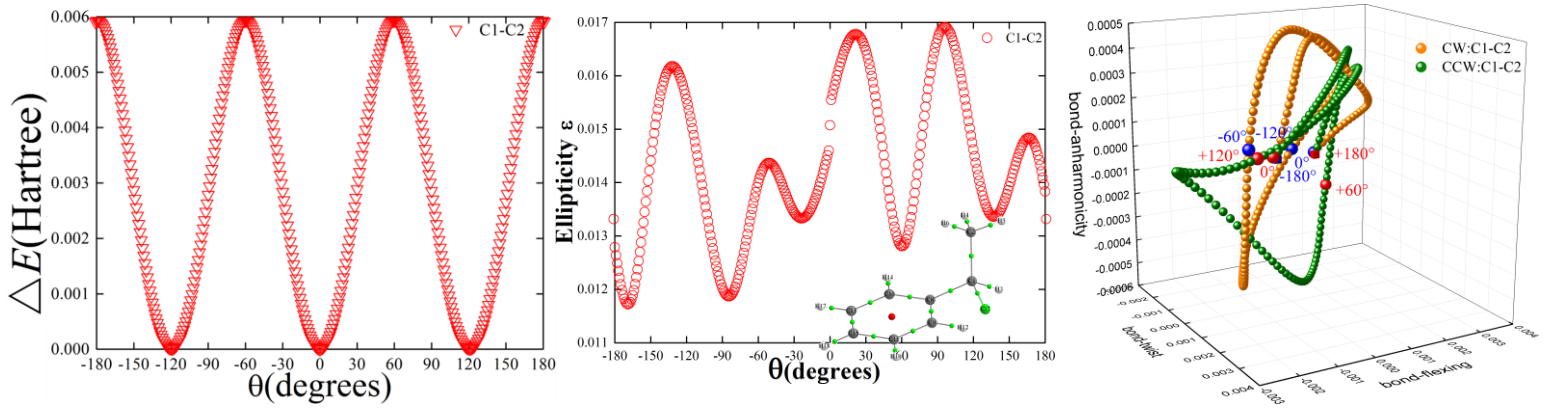

Figure S3(f): The variation of the relative energy ΔE (in a.u.) of the S stereoisomer of 1-chloro-1-phenylethane (left panel) with the torsion θ. The corresponding variation of the ellipticity ε (middle panel), with the (S)-1-chloro-1-phenylethane molecular graph (inset panel). The (S)-1-chloro-1-phenylethane stress tensor trajectories $T_\sigma(s)$ (right panel) of the torsional C1-C2 *BCP*, see the caption of **Figure S3(a)**.

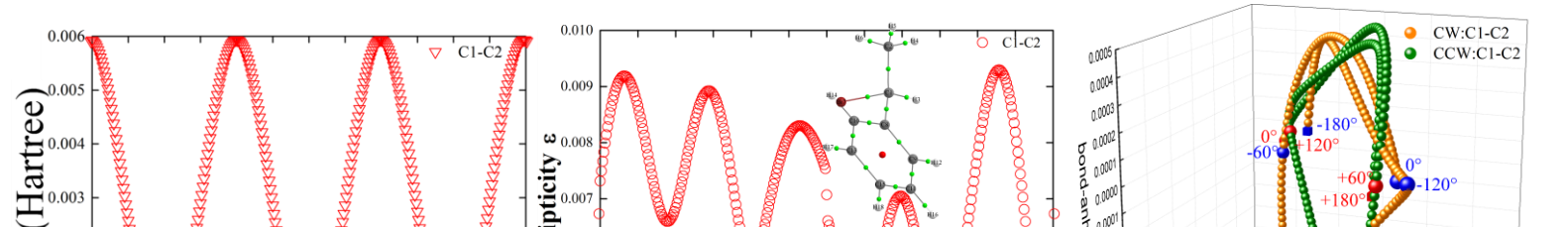

Figure S3(g): The variation of the relative energy ΔE (in a.u.) of the R stereoisomer of 1-bromo-1-phenylethane (left panel) with the torsion θ. The corresponding variation of the ellipticity ε (middle panel), with the (R) 1-bromo-1-phenylethane molecular graph (inset panel). The (R)-1-bromo-1-phenylethane stress tensor trajectories $T_\sigma(s)$ (right panel) of the torsional C1-C2 *BCP*, see the caption of **Figure S3(a)**.

4. Supplementary Materials S4. $T_\sigma(s)$ of the torsional C1-C2 *BCP* of ethane and substituted ethane.

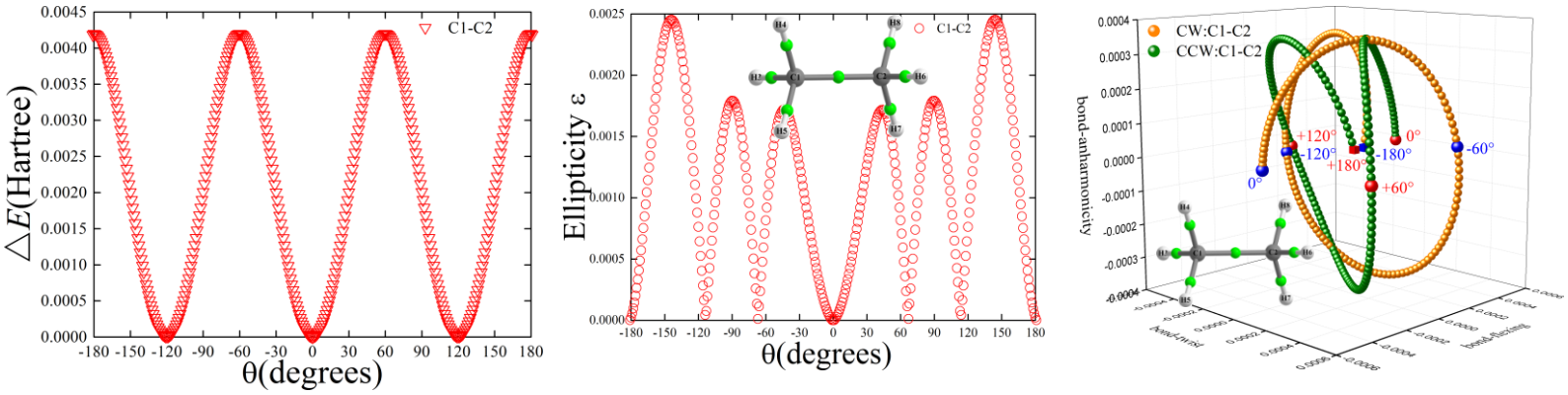

Figure S4(a): The variation of the relative energy ΔE (in a.u.) of the ethane (left panel) with the torsion θ, clockwise (CW) and counterclockwise (CCW) -180.0° ≤ θ ≤ +180.0° directions. The corresponding variation of the ellipticity ε (middle panel) with the ethane molecular graph (inset panel), with the green spheres indicate the bond critical points (*BCP*s). The ethane stress tensor trajectories $T_\sigma(s)$ (right panel) of the torsional C1-C2 *BCP* for the CW and CCW directions of torsion.

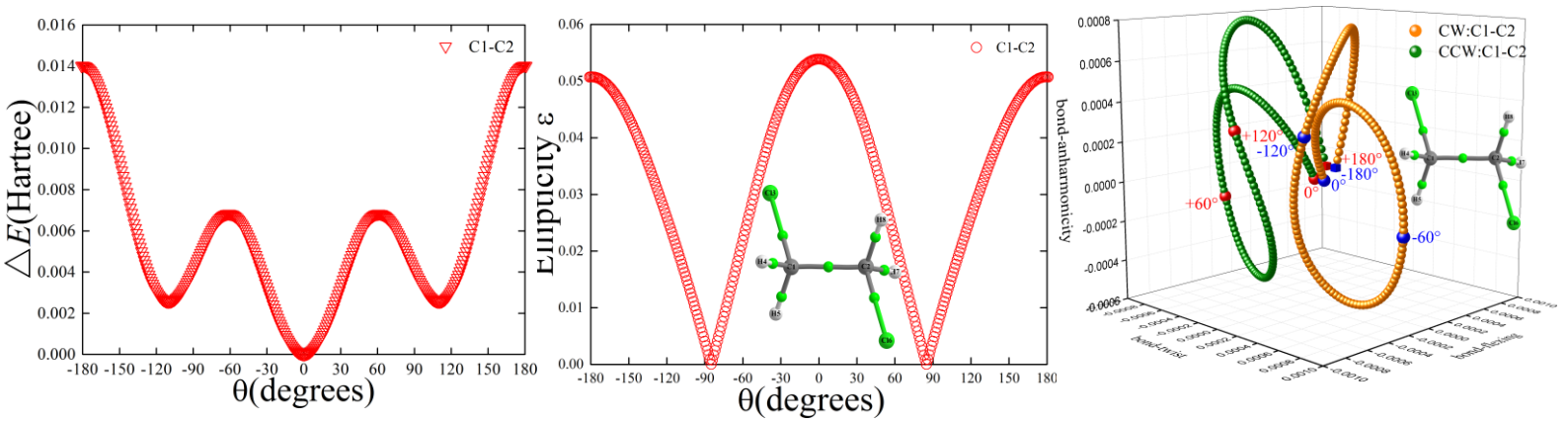

Figure S4(b): The variation of the relative energy ΔE (in a.u.) of 1,2 dichloroethane (left panel) with the torsion θ, CW and CCW directions. The corresponding variation of the ellipticity ε (middle panel), with the 1,2 dichloroethane molecular graph (inset panel). The 1,2 dichloroethane stress tensor trajectories $T_\sigma(s)$ (right panel) of the torsional C1-C2 *BCP* for the CW and CCW directions of torsion.

Table S4(a). For achiral molecules, the maximum stress tensor projections {bond-twist$_{max}$, bond-flexing$_{max}$, bond-anharmonicity$_{max}$} for the torsional C1-C2 *BCP*, where **dr** is a finite *BCP* shift vector, see the caption of **Figure S4(a)** for further details.

	{bond-twist$_{max}$, bond-flexing$_{max}$, bond-anharmonicity$_{max}$}	
	CW	**CCW**
Molecule		
ethane	{0.71936, 0.81808, 0.697984}	{0.77078, 0.72315, 0.697987}
1,2 dichloroethane	{0.86558, 0.61238, 1.324024}	{0.86547, 0.61230, 1.324019}

Table S4(b). For achiral molecules, the values of the chirality C_σ, the helicity B_σ and of the *chirality-helicity* function $C_{helicity}$ = (chirality C_σ)(helicity B_σ) are tabulated, see also **Table S4(a)**.

Molecule	{C_σ, B_σ}	$C_{helicity}$	[C_σ,B_σ]
ethane	{0.051421**[S_σ]**, 0.000003**[S_σ]**}	≈ 0 (1.5x10^{-7})	**[S_σ,S_σ]**
1,2 dichloroethane	{-0.000114 **[R_σ]**, -0.000005**[R_σ]**}	≈ 0 (6.0x10^{-10})	**[R_σ,R_σ]**

5. Supplementary Materials S5. $T_\sigma(s)$ of the torsional C1-C2 *BCP* of ethene, substituted ethene

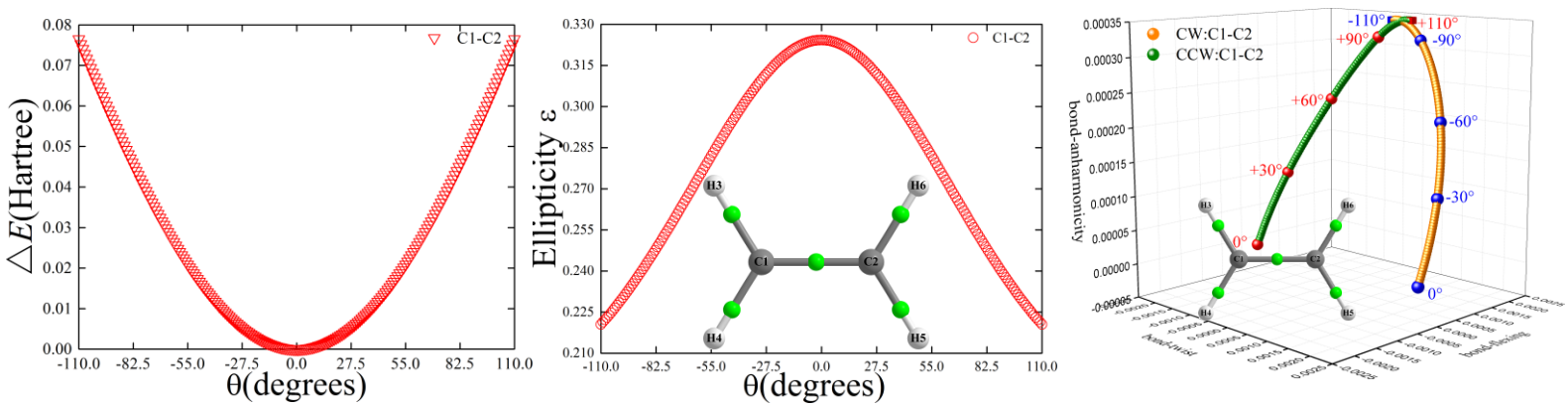

Figure S5(a): The variation of the relative energy ΔE (in a.u.) of the ethene (left panel) with the torsion θ, clockwise (CW) and counterclockwise (CCW) -110.0° ≤ θ ≤ +110.0° directions. The corresponding variation of the ellipticity ε (middle panel) with the ethene molecular graph (inset panel), with the green spheres indicate the bond critical points (*BCP*s). The ethene stress tensor trajectories $T_\sigma(s)$ (right panel) of the torsional C1-C2 *BCP* for the CW and CCW directions of torsion.

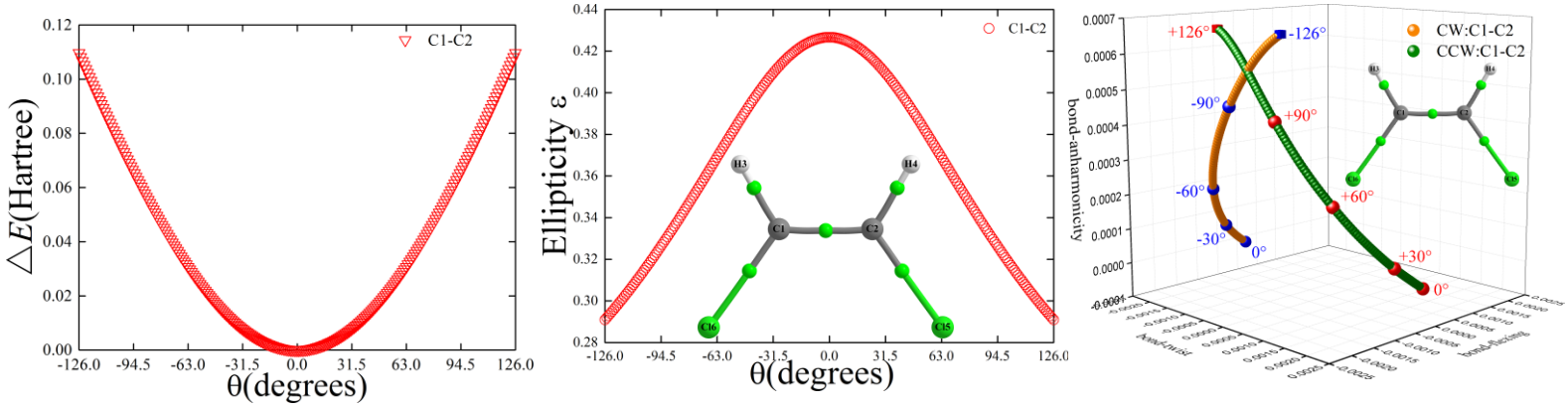

Figure S5(b): The variation of the relative energy ΔE (in a.u.) of cis-1,2 dichloroethene (left panel) with the torsion θ, clockwise (CW) and counterclockwise (CCW) -126.0° ≤ θ ≤ +126.0° directions. The corresponding variation of the ellipticity ε (middle panel), with the cis-1,2 dichloroethene molecular graph (inset panel) where the green spheres indicate the bond critical points (*BCP*s). The cis-1,2 dichloroethene stress tensor trajectories $T_\sigma(s)$ (right panel) of the torsional C1-C2 *BCP* for the CW and CCW directions of torsion.

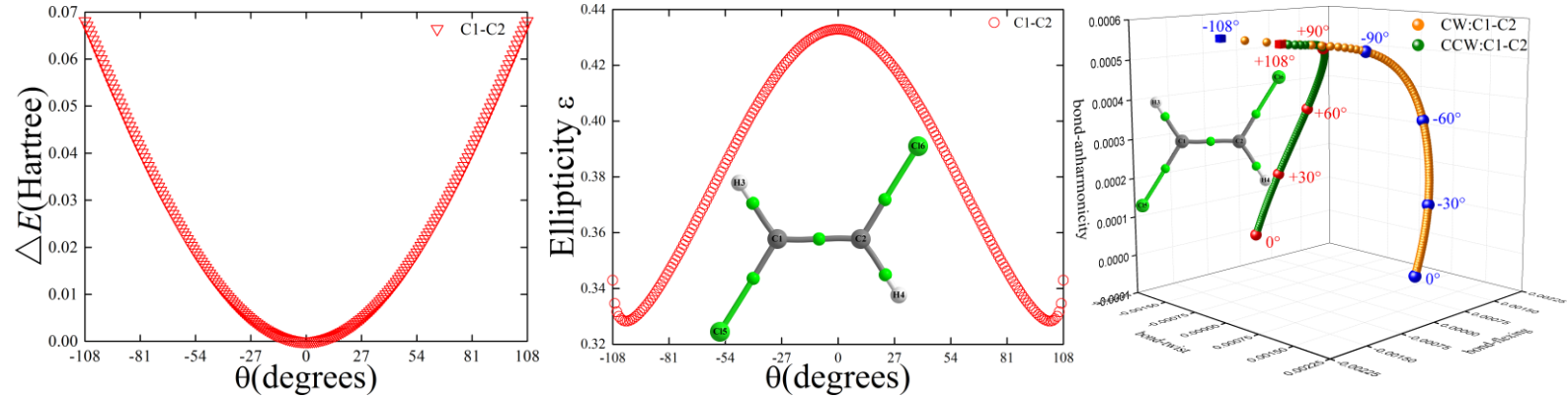

Figure S5(c): The variation of the relative energy ΔE (in a.u.) of trans-1,2 dichloroethene (left panel) with the torsion θ, CW and CCW directions. The corresponding variation of the ellipticity ε (middle panel), with the trans-1,2 dichloroethene molecular graph (inset panel) where the green spheres indicate the bond critical points (*BCP*s). The trans-1,2 dichloroethene stress tensor trajectories $T_\sigma(s)$ (right panel) of the torsional C1-C2 *BCP* for the CW and CCW directions of torsion.

Table S5(a). For achiral molecules, the maximum stress tensor projections {bond-twist$_{max}$, bond-flexing$_{max}$, bond-anharmonicity$_{max}$} for the torsional C1-C2 *BCP*, where **dr** is a finite *BCP* shift vector, see the caption of **Figure 2** for further details.

	{bond-twist$_{max}$, bond-flexing$_{max}$, bond-anharmonicity$_{max}$}	
	CW	**CCW**
Molecule		
ethene	{2.29396, 1.84450, 0.34564}	{2.29293, 1.84449, 0.34584}
cis-1,2 dichloroethene	{3.00691, 1.85863, 0.68446}	{3.00693, 1.85864, 0.68445}
trans-1,2 dichloroethene	{2.51790, 2.50190, 0.56300}	{2.51690, 2.50210, 0.56310}

Table 5(b). For achiral molecules, the values of the chirality C_σ, the helicity B_σ and of the *chirality-helicity* function $C_{helicity}$ = (chirality C_σ)(helicity B_σ) are tabulated, see also **Table 5(a)**. The connectivity *n* of the fixed reference C1 atom is indicated.

Molecule	{C_σ, B_σ}	$C_{helicity}$	[$C_\sigma B_\sigma$]
ethene	{-0.00103**[R_σ]**, 0.000200**[S_σ]**}	≈ 0 (-2.1x10^{-7})	**[$R_\sigma S_\sigma$]**
cis-1,2 dichloroethene	{0.000018**[S_σ]**,-0.000011**[R_σ]**}	≈ 0 (-2.0x10^{-10})	**[$S_\sigma R_\sigma$]**
trans-1,2 dichloroethene	{-0.00100**[R_σ]**, 0.000100**[S_σ]**}	≈ 0 (1.0x10^{-7})	**[$R_\sigma S_\sigma$]**